PHYSICAL REVIEW D **93,** 115035 (2016)

LHC signals of a $B-L$ supersymmetric standard model *CP*-even Higgs boson

A. Hammad,[1] S. Khalil,[1] and S. Moretti[2]

[1]*Center for Fundamental Physics, Zewail City of Science and Technology, 6 October City, 12588 Giza, Egypt*
[2]*School of Physics & Astronomy, University of Southampton, Highfield, Southampton SO17 1BJ, United Kingdom*

(Received 16 April 2016; published 27 June 2016)

We study the scope of the Large Hadron Collider in accessing a neutral Higgs boson of the $B-L$ supersymmetric standard model. After assessing the surviving parameter space configurations following the Run 1 data taking, we investigate the possibilities of detecting this object during Run 2. For the model configurations in which the mixing between such a state and the discovered standard-model-like Higgs boson is non-negligible, there exist several channels enabling its discovery over a mass range spanning from ≈140 to ≈500 GeV. For a heavier Higgs state, with mass above 250 GeV (i.e., twice the mass of the Higgs state discovered in 2012), the hallmark signature is its decay in two such 125 GeV scalars, $h' \to hh$, where $hh \to b\bar{b}\gamma\gamma$. For a lighter Higgs state, with mass of order 140 GeV, three channels are accessible: $\gamma\gamma$, $Z\gamma$, and ZZ, wherein the Z boson decays leptonically. In all such cases, significances above discovery can occur for already planned luminosities at the CERN machine.

DOI: 10.1103/PhysRevD.93.115035

I. INTRODUCTION

After the Higgs boson discovery at the Large Hadron Collider (LHC) during Run 1, a new era in particle physics has begun. While precision measurements of the detected state as reported by the ATLAS and CMS collaborations (now also including Run 2 data) confirm a standard-model-like nature with a rather light mass of ≈125 GeV, significant effort is now being put forth in the search for companion Higgs states, as any construct beyond the standard model (BSM) embedding a Higgs mechanism is likely nonminimal; i.e., it would include new Higgs bosons in its spectrum. In the myriad of BSM scenarios available, a special place is held by models of supersymmetry (SUSY), wherein the lightest SM-like Higgs boson mass is naturally limited to be at the electroweak (EW) scale (say below $2M_W$) and where one also finds additional (neutral) Higgs bosons. Thus, one may well be tempted to conclude that a SUSY scenario may be behind the aforementioned data.

Amongst the many SUSY realizations studied so far, though, one really ought to single out those that also offer explanations for other data pointing to BSM physics, chiefly those indicating that neutrinos oscillate, and hence that they have mass. One is therefore well motivated in looking at the $B-L$ supersymmetric standard model (BLSSM). The BLSSM is an extension of the time-honoured minimal supersymmetric standard model (MSSM) obtained by adopting a further $U(1)_{B-L}$ gauge group alongside the SM structure, i.e., $SU(3)_C \times SU(2)_L \times U(1)_Y \times U(1)_{B-L}$. [This requires an additional Higgs singlet field to break the new $U(1)_{B-L}$ symmetry, in turn releasing an additional Z' state as well.] The particle content of the BLSSM, limited to its Higgs sector, includes three additional neutral Higgs fields (henceforth h', H', and A') with respect to the MSSM ones (henceforth h, H, and A) [1].

The enriched Higgs sector of the BLSSM, with respect to the MSSM one, offers the possibility of relieving the deadlock typical of the minimal SUSY model, wherein a light SM-like Higgs state (the h boson at ≈125 GeV) requires the other Higgs states (H and A in particular) to be much heavier in comparison (and moderately coupled to SM matter fermions and gauge bosons). This does not necessarily occur in the BLSSM, as the h', H', and A' states can have a singlet component sufficient to render them very lightly mixed with the h one, thereby allowing at the same time sizable couplings to SM objects and the possibility that their mass, depending on the vacuum expectation value (VEV) of the Higgs singlet field, is significantly lighter than those of the MSSM-like H and A particles.

In fact, a natural configuration of the BLSSM is to find alongside the above SM-like Higgs state another rather light physical Higgs boson, h', also CP-even, with a mass $m_{h'} \geq 135$ GeV. This fact was exploited in Refs. [2–4] to explain potential Run 1 signals for another Higgs boson, i.e., h', in the $h' \to ZZ^* \to 4l$ (wherein a 2σ excess is appreciable in the vicinities of 145 GeV [5]), $h' \to \gamma\gamma$ (prompting a 2.9σ excess around 137 GeV [6]), and $h' \to Z\gamma$ (yielding a 2σ excess around 140 GeV [7]) decay modes.

As new data are presently being collected at Run 2, we revisit here the scope of the LHC in confirming or disproving the above hypothesis of additional light Higgs boson signals. Furthermore, thanks to the higher energy and luminosity afforded by the new CERN machine configuration, we also investigate the possibilities of

accessing a heavier h' state, with a mass up to 500 GeV or so. Our paper is organized as follows. In the next section, we introduce the Higgs boson spectrum in the BLSSM. In Secs. III and IV we describe our analysis of the light and heavy mass ranges, respectively, of the h' state. We conclude in Sec. V.

II. HIGGS BOSONS IN THE BLSSM

The BLSSM model consists of, in addition to the MSSM particle content, two SM singlet chiral Higgs superfields $\chi_{1,2}$ and three SM singlet chiral superfields, $\nu_i, i = 1, 2, 3$ [8]. The superpotential of this model is given by

$$W = Y_u \hat{Q}\hat{H}_u\hat{U}^c + Y_d\hat{Q}\hat{H}_d\hat{D}^c + Y_e\hat{L}\hat{H}_d\hat{E}^c + Y_\nu\hat{L}\hat{H}_u\hat{\nu}^c + Y_\nu\hat{\nu}\,\hat{l}\,\hat{H}_u. + \mu\hat{H}_u\hat{H}_d + \mu'\hat{\chi}_1\hat{\chi}_2. \quad (1)$$

The corresponding soft SUSY breaking terms and the details of the associated spectrum can be found in Refs. [8,9]. Note that the $U(1)_Y$ and $U(1)_{B-L}$ gauge kinetic mixing can be absorbed in the covariant derivative redefinition and, in this basis, one finds

$$M_Z^2 = \frac{1}{4}(g_1^2 + g_2^2)v^2, \quad (2)$$

$$M_{Z'}^2 = g_{BL}^2 v'^2 + \frac{1}{4}\tilde{g}^2 v^2, \quad (3)$$

where g_{BL} is the gauge coupling of $U(1)_{B-L}$ and $\tilde{g}$ is the gauge coupling mixing between $U(1)_Y$ and $U(1)_{B-L}$. In addition, $v = \sqrt{v_1^2 + v_2^2} \simeq 246$ GeV, $v' = \sqrt{v_1'^2 + v_2'^2} \simeq \mathcal{O}(1)$ TeV are the VEVs of the Higgs fields H_i and χ_i, respectively.

A. The spectrum

The neutral Higgs boson masses are obtained by making the usual redefinition of the Higgs fields, i.e., $H_{1,2}^0 = \frac{1}{\sqrt{2}}(v_{1,2} + \sigma_{1,2} + i\phi_{1,2})$ and $\chi_{1,2}^0 = \frac{1}{\sqrt{2}}(v'_{1,2} + \sigma'_{1,2} + i\phi'_{1,2})$, where $\sigma_{1,2} = \mathrm{Re}H_{1,2}^0$, $\phi_{1,2} = \mathrm{Im}H_{1,2}^0$, $\sigma'_{1,2} = \mathrm{Re}\chi_{1,2}^0$, and $\phi'_{1,2} = \mathrm{Im}\chi_{1,2}^0$. The real parts correspond to the CP-even Higgs bosons and the imaginary parts correspond to the CP-odd Higgs bosons. Therefore, the squared matrix of the BLSSM CP-even neutral Higgs fields at tree level, in the basis $(\sigma_1, \sigma_2, \sigma'_1, \sigma'_2)$, is given by

$$M^2 = \begin{pmatrix} M_{hH}^2 & M_{hh'}^2 \\ M_{hh'}^{2^T} & M_{h'H'}^2 \end{pmatrix}, \quad (4)$$

where M_{hH}^2 is the usual MSSM neutral CP-even Higgs mass matrix, which leads to a SM-like Higgs boson with mass, at one-loop level, of order 125 GeV and a heavy Higgs boson with mass $m_H \sim \mathcal{O}(1\ \mathrm{TeV})$. In addition, the BLSSM matrix $M_{h'H'}^2$ is given by

$$M_{h'H'}^2 = \begin{pmatrix} m_{A'}^2 c_{\beta'}^2 + g_{BL}^2 v_1'^2 & -\frac{1}{2}m_{A'}^2 s_{2\beta'} - g_{BL}^2 v'_1 v'_2 \\ -\frac{1}{2}m_{A'}^2 s_{2\beta'} - g_{BL}^2 v'_1 v'_2 & m_{A'}^2 s_{\beta'}^2 + g_{BL}^2 v_2'^2 \end{pmatrix}, \quad (5)$$

where $c_x = \cos(x)$ and $s_x = \sin(x)$. Therefore, the eigenvalues of this mass matrix are given by

$$m_{h',H'}^2 = \frac{1}{2}\Big[(m_{A'}^2 + M_{Z'}^2) \mp \sqrt{(m_{A'}^2 + M_{Z'}^2)^2 - 4m_{A'}^2 M_{Z'}^2 \cos^2 2\beta'}\Big]. \quad (6)$$

If $\cos^2 2\beta' \ll 1$, one finds that the lightest $B - L$ neutral Higgs state is given by

$$m_{h'} \simeq \left(\frac{m_{A'}^2 M_{Z'}^2 \cos^2 2\beta'}{m_{A'}^2 + M_{Z'}^2}\right)^{\frac{1}{2}} \simeq \mathcal{O}(100\ \mathrm{GeV}). \quad (7)$$

The mixing matrix $M_{hh'}^2$ is proportional to $\tilde{g}$ and, for a gauge coupling $g_{BL} \sim |\tilde{g}| \sim \mathcal{O}(0.1)$, these off-diagonal terms are about one order of magnitude smaller than the diagonal ones. However, they are still crucial for generating interaction vertices between the light BLSSM Higgs boson, h', and the MSSM-like Higgs state, h.

The CP-even neutral Higgs mass matrix in Eq. (4) can be diagonalized by a unitary transformation:

$$\Gamma M^2 \Gamma^\dagger = \mathrm{diag}\{m_h^2, m_{h'}^2, m_H^2, m_{H'}^2\}. \quad (8)$$

A numerical scan confirms that, while $\tan'\beta \leq 1.2$, the h' state can be the second Higgs boson mass, whereas the other two CP-even states H, H' are heavy. Also, the mixings Γ_{ij} are proportional to $\tilde{g}$ and they vanish (at tree level) if $\tilde{g} = 0$. In this regard, h' can be written in terms of gauge eigenstates as

$$h' = \Gamma_{21}\sigma_1 + \Gamma_{22}\sigma_2 + \Gamma_{23}\sigma'_1 + \Gamma_{24}\sigma'_2. \quad (9)$$

Thus, the couplings of the h' with up- and down-quarks are given by

$$g_{h'u\bar{u}} = -i\frac{m_u \times \Gamma_{22}}{v \sin\beta}, \quad (10)$$

$$g_{h'd\bar{d}} = -i\frac{m_d \times \Gamma_{21}}{v \cos\beta}. \quad (11)$$

Similarly, one can derive the h' couplings with the W^+W^- and ZZ gauge boson pairs:

$$g_{h'WW} = ig_2 M_W(\Gamma_{22}\sin\beta + \Gamma_{21}\cos\beta),$$
$$g_{h'ZZ} = \frac{i}{2}[4g_{BL}\sin^2\theta'(v_1'\Gamma_{22} + v_2'\Gamma_{21}) + (v_2\Gamma_{22} + v_1\Gamma_{21})(g_z\cos\theta' - \tilde{g}\sin\theta')^2], \quad (12)$$

where $g_z = \sqrt{g_1^2 + g_2^2}$ and θ' is the mixing angle between Z and Z'. Since $\sin\theta' \ll 1$ (as per experimental constraints), the coupling of the h' with ZZ, $g_{h'ZZ}$, will be as follows:

$$g_{h'ZZ} \simeq ig_z M_Z(\Gamma_{22}\sin\beta + \Gamma_{21}\cos\beta). \quad (13)$$

In Fig. 1 we show the h' (in Γ_{21}, Γ_{22}) and h (in Γ_{11}, Γ_{12}) decompositions. Note that, if $\tilde{g} = 0$, the coupling of the BLSSM lightest Higgs boson with the SM particles vanishes at tree level and is very suppressed [$\sim\mathcal{O}(10^{-6})$] at loop level. Here we choose a parameter space such that the lightest chargino is rather light, $M_{\chi^\pm} = 120$ GeV, so as to enhance the SUSY contributions to the Higgs decays into $\gamma\gamma$ and $Z\gamma$; namely, we consider a low $\tan\beta$ between 1.1 and 5 and μ and M_2 between 100 and 300 GeV, while other SUSY mass and trilinear parameters are assumed to be of order few TeV. It is worth mentioning that the dominant decomposition for the SM-like Higgs state is $\Gamma_{12} \sim \mathcal{O}(1)$, which is equivalent to $\sin\beta \sim \mathcal{O}(1)$ in the MSSM, and that the light BLSSM Higgs, h', is dominated by Γ_{23} and $\Gamma_{24} \sim \mathcal{O}(0.5)$.

We display in Fig. 2 the branching ratios (BRs) of h' into all its possible decay channels, for nonzero $\tilde{g}$, including gg, $\gamma\gamma$, and $Z\gamma$ that are induced at one-loop level. A few remarks on this figure are in order: (i) for $m_{h'} \geq 200$ GeV, h' decays are dominated by the W^+W^- and hh channels; (ii) in the BLSSM the BR$(h' \to Z\gamma)$ is typically larger than the BR$(h' \to \gamma\gamma)$, unlike the MSSM and SM where it is the other way around.

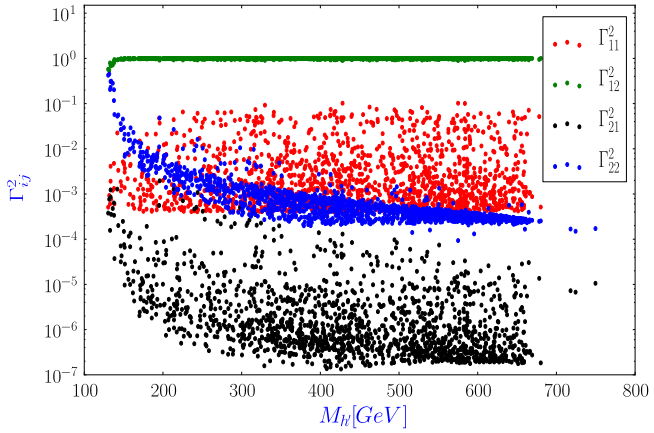

FIG. 1. Decomposition of the BLSSM Higgs boson, h', and the SM-like Higgs, h, versus $M_{h'}$.

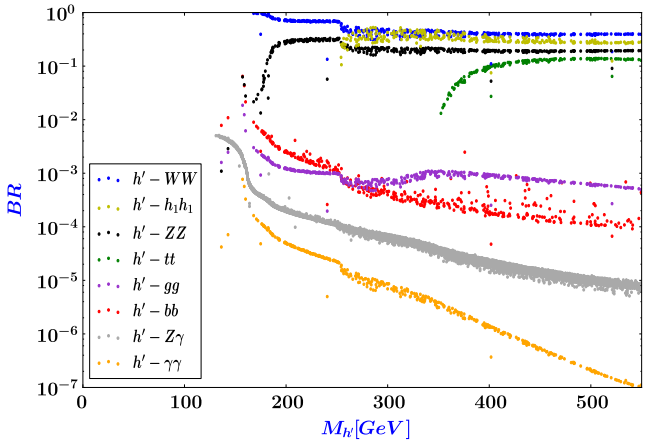

FIG. 2. The BRs of h' versus $M_{h'}$ for $0.1 \leq \tilde{g} \leq 0.25$ and $g_{BL} = 0.5$.

B. Implementation and simulation

The Higgs production modes included in our forthcoming numerical analysis are gluon-gluon fusion (ggF), which induces around 90% of the total cross section (hereafter denoted by σ), while vector-boson fusion (VBF), Higgs-strahlung (VH) and associated production with top quarks (ttH) contribute with around 10%. The data analyses in these channels are based on an integrated luminosity of 20 fb^{-1} at $\sqrt{s} = 7$, 8 TeV and expected to rely upon from 100 to $\mathcal{O}(1000)$ fb^{-1} at $\sqrt{s} = 13$ TeV. The magnitude of the signal is usually expressed via the "signal strength" parameters, defined as

$$\mu_{XY} = \frac{\sigma(pp \to h' \to XY)}{\sigma(pp \to h \to XY)^{\rm SM}} = \frac{\sigma(pp \to h')}{\sigma(pp \to h)^{\rm SM}} \times \frac{\mathrm{BR}(h' \to XY)}{\mathrm{BR}(h \to XY)^{\rm SM}}. \quad (14)$$

Herein, the h' in the numerator is indeed the lightest BLSSM CP-even state and the h in the denominator is the SM Higgs boson with mass 125 GeV whereas in both cases the cross section is intended as computed inclusively (i.e., over the ggF, VBF, VH, and ttH modes [10]).

For the implementation of the BLSSM we used SARAH [11] and SPheno [12] to build the model. For loop induced channels we linked it with CP-SuperH [13]. The matrix-element calculation and events generation were derived by MadGraph [14]. We then used Pythia [15] to simulate the initial- and final-state radiation, fragmentation, and hadronization effects. For detector simulation we passed the Pythia output to Delphes [16]. For data analysis, we used MadAnalysis5 [17].

In our scans, for the computation of the signal strength distributions in the next section, we consider the following regions of the parameter space:

$$m_0 = 1\text{–}3\ \text{TeV}, \qquad M_3 = 3\ \text{TeV},$$
$$M_2 = 120\text{–}300\ \text{GeV}, \qquad M_1 = 100\text{–}500\ \text{GeV},$$
$$\tan\beta = 5, \qquad \tan\beta' = 1.15,$$
$$|A_0| = 1.5\text{–}3\ \text{TeV}, \qquad \mu = 100\text{–}350\ \text{GeV},$$
$$|\tilde{g}| = 0.1\text{–}0.25, \qquad g_{BL} = 0.5. \tag{15}$$

In addition, in the upcoming event generation analyses, the following benchmark point is assumed:

$$m_{\chi_1^+} = 120\ \text{GeV}, \qquad \mu = 120\ \text{GeV}, \qquad \tan\beta = 5,$$
$$\tan\beta' = 1.15, \qquad \tilde{g} = -0.24, \qquad g_{BL} = 0.5, \tag{16}$$

while all other SUSY particles are of order TeV. This benchmark point is consistent with current theoretical and experimental limits, as we determined through an independent program checked against specialized literature. It is worth pointing out that light μ and chargino mass are crucial for enhancing the SUSY contributions to $h \to \gamma\gamma$ and $h \to Z\gamma$ simultaneously. Finally, notice that the h' masses considered below (140, 300, 350, and 480 GeV) are all accessible through the inputs in Eq. (16), upon suitable adjustments of the Higgs potential parameters.

III. SEARCH FOR A HEAVY BLSSM HIGGS BOSON AT THE LHC

In this section we analyze possible signatures of the lightest genuine BLSSM scalar boson h' when it is rather heavy, with mass between 300 GeV and 1 TeV, at Run 2 of the LHC. Figure 2 shows that the decay channels available to the h' state are the same as those of the SM-like h one, with the notable exception of the former decaying into (pairs of) the latter, i.e., $h' \to hh$. The corresponding BR can be in fact the dominant one, once its threshold is open. It is therefore the distinctive feature of a heavy h' whenever $m_{h'} \geq 2m_h$.

ATLAS [18] and CMS [19] have both recently searched for hh signals decaying to a $4b$ final state. However, it turned out to be a significant challenge to distinguish the emerging signature, made of four b-jets in the final state, from the huge multijet QCD background. In fact, the sensitivity achieved by the LHC experiments was rather poor and results obtained were consistent with the SM. We shall nonetheless attempt to extract this signal, so as to compare the scope of detecting it at Run 2 versus what has been achieved at Run 1.

The decay $h' \to hh \to \gamma\gamma b\bar{b}$, which has been experimentally analyzed in Refs. [20,21], may prove to be the best way to probe a heavy h' of the BLSSM, since the problem of a suppressed $h \to \gamma\gamma$ decay is offset by the fact that both $h' \to hh$ and $h \to b\bar{b}$ are the dominant decays of the two Higgs states concerned. The aforementioned searches were performed on the $\sqrt{s} = 8$ TeV data set corresponding to an integrated luminosity of $\approx 20\ \text{fb}^{-1}$. Following these, the ATLAS Collaboration observed five excess events (above and beyond the expected SM yield) within a mass windows from 260 to 500 GeV, which represent an excess of 2.4σ, with an intriguing p_0-value (local probability of compatibility with the background) $\sim 10^{-3}$ at 300 GeV, which corresponds to 3.0σ [20]. In contrast, CMS reported that searches within the mass region from 260 GeV to 1100 GeV were consistent with expectations from SM processes [21]. Needless to say then, we will thoroughly investigate this signature too in the upcoming Run 2.

Before proceeding to do so in two separate subsections, let us start by explaining how such large decay rates for $h' \to hh$ can occur in the BLSSM. Herein, the scalar trilinear coupling between h' and hh is given by

$$\lambda_{h'hh}^{\text{BLSSM}} = \frac{-i\tilde{g}g_{BL}}{4}\Gamma_{i2}^2(2v_2'\Gamma_{24} - v_1'\Gamma_{23}). \tag{17}$$

Here we have assumed, as advocated in the previous section, that $\Gamma_{12} \gg \Gamma_{11,13,14}$ and $\Gamma_{23,24} \gg \Gamma_{21,22}$. This should be compared with the MSSM trilinear scalar coupling

$$\lambda_{Hhh}^{\text{MSSM}} = -i\frac{g_1^2 + g_2^2}{4}v[2\sin 2\alpha \sin(\beta + \alpha) - \cos 2\alpha \cos(\beta + \alpha)], \tag{18}$$

for which, when $\sin\beta > \cos\beta$ and assuming the decoupling limit where $\alpha \sim \beta$, one finds

$$\lambda_{Hhh}^{\text{MSSM}} = -i\frac{g_1^2 + g_2^2}{4}v\sin^3\beta. \tag{19}$$

Also note that the Hhh coupling is modified in the BLSSM with respect to the MSSM and takes the form

$$\lambda_{Hhh}^{\text{BLSSM}} = \frac{i}{4}(g_1^2 + \tilde{g}^2 + g_2^2)\Gamma_{31}(v_d\Gamma_{12}^2 + 2v_u\Gamma_{12}\Gamma_{11})). \tag{20}$$

It is clear that $\lambda_{h'hh}^{\text{BLSSM}} \propto v_{1,2}' \sim \mathcal{O}(1)$ TeV is much larger than the coupling Hhh in either SUSY model, which is of order of the EW scale. Therefore, one would expect that the decay rate of $h' \to hh$ is always much larger than that of $H \to hh$.

A. The $hh \to 4b$ decays of a heavy BLSSM Higgs boson

The total cross section for the aforementioned $4b$ final state is given by

$$\sigma(pp \to h' \to hh \to 4b) = \sigma(pp \to h') \times \text{BR}(h' \to hh) \times \text{BR}(h \to b\bar{b})^2, \tag{21}$$

and is dominated by ggF, which is in turn obtained as (for a CM energy of 13 TeV)

$$\sigma(pp \to h) \times \Gamma_{22}^2 \simeq \mathcal{O}(1)\ \text{pb} \tag{22}$$

while, for $m_{h'} \simeq 350$ GeV, the $\text{BR}(h' \to hh) \sim 0.5$ and the $\text{BR}(h \to b\bar{b}) \sim 0.6$, as can be seen from Fig. 2. Thus, one finds that $\sigma(pp \to h' \to hh \to 4b)$ in the BLSSM $\sim 10^{-1}$ pb. Despite the high total cross section, the huge contribution from background b-jet radiation exceeds the signal, so that the associated events do not appear as significant over the SM background. This conclusion is confirmed by Fig. 3, where we show the number of events of signal with its irreducible background as a function of the invariant mass of the four b-jets, M_{4b}. Note that we used the b-tagging algorithm included in MadAnalysis [17], so that a jet is identified as originating from a b-quark when it can be matched to it once it lies within a cone of a certain radius R around one of the parton-level b-quarks, this yielding an efficiency of about 65%.

Here, we considered the cuts applied in [22]; i.e., candidate events are required to have at least four b-tagged jets, each with $p_T \geq 40$ GeV and separated by a cone of $\Delta R = 1.5$. However, as can be seen from the plot, the signal is well below the background. The highest background contribution comes from a mutijet's final state, followed by $t\bar{t}$ production and (semi)hadronic (anti)top decays, which gives about 22% of the noise, while the reducible background contributions come from "Z + jets," ZZ and Zh, and are found to contribute less than 1%.

The signal distribution is presented for $m'_h \approx 2m_t \approx$ 350 GeV, which is in fact the worst-case scenario, as this is where the $t\bar{t}$ background peaks in M_{4b}. However, we have tried different $m_{h'}$ values, to no avail, in the mass range from 300 GeV to 1 TeV. The signal would never be accessible, either with standard or with upgraded luminosities.

B. The $hh \to b\bar{b}\gamma\gamma$ decays of a heavy BLSSM Higgs boson

Now we turn to the process $pp \to h' \to hh \to \gamma\gamma b\bar{b}$. Although this mode has smaller cross section than $\sigma(pp \to h' \to hh \to 4b)$, it is more promising due to the clean diphoton trigger with excellent mass resolution and low background contamination. This is confirmed in Fig. 4, where the number of signal events is displayed versus the background as a function of the invariant mass $M_{\gamma\gamma bb}$ for two examples of h' masses: $m'_h = 300$ GeV and $m_{h'} = 480$ GeV.

The background to this process can be classified into two categories: background events containing a real Higgs boson decay, $h \to \gamma\gamma$ and $h \to bb$, and the continuum background of events not containing a Higgs boson. The continuum contribution in the signal region is split between events with two photons and events with a single photon in association with a jet faking the second photon. Further, the two b-tagged jets include real heavy-flavor jets as well as mistagged light-flavor jets and gluons. The contribution from dileptonic decays of $t\bar{t}$ events where two electrons fake the two photons is roughly 10% of the total background. The contribution from other processes, like leptonic decays of digauge bosons where two electrons fake the two photons and the Higgs boson comes associated with a W/Z, is negligible. In our analysis, we adopt the following acceptance cuts in transverse momentum, pseudorapidity of and separation amongst the photons and jets:

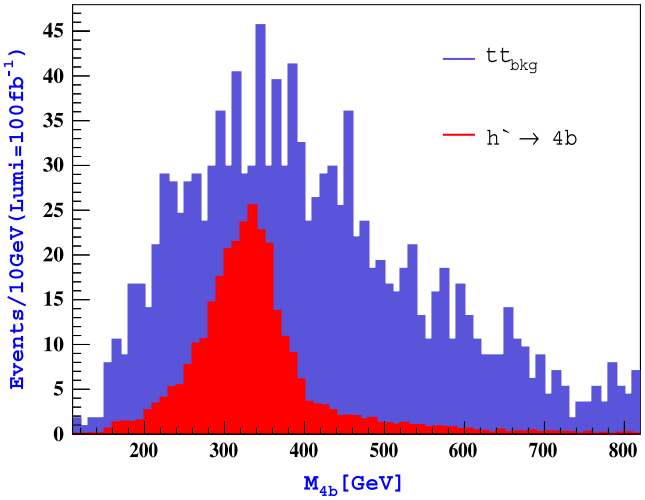

FIG. 3. Number of signal events for $h' \to hh \to 4b$ decays (red) induced by ggF and VBF versus the $4b$ invariant mass at $\sqrt{s} =$ 13 TeV after 100 fb^{-1} of luminosity alongside the $t\bar{t}$ background (blue). (The huge multijet background, which is given in Ref. [22], is not shown.) Here, $m_{h'} = 350$ GeV.

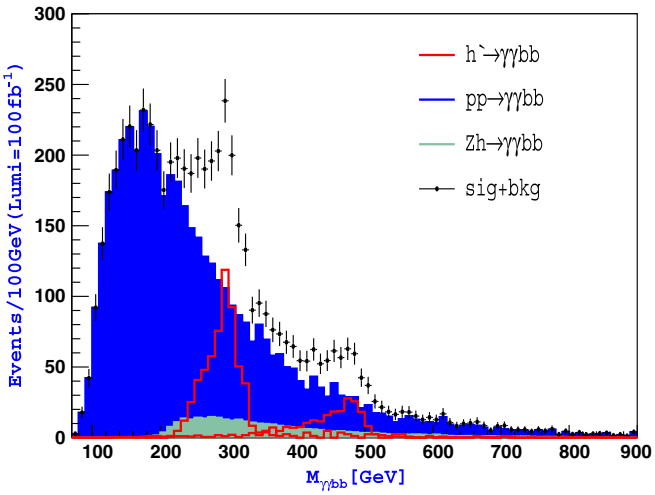

FIG. 4. Number of signal events for $h' \to \gamma\gamma b\bar{b}$ decays (red) induced by ggF and VBF versus the $\gamma\gamma b\bar{b}$ invariant mass at $\sqrt{s} =$ 13 TeV after 100 fb^{-1} of luminosity alongside the two dominant $\gamma\gamma$ (blue) and Zh (green) backgrounds. Their sum is also shown as data points. Here, $m'_h = 300$ and 480 GeV.

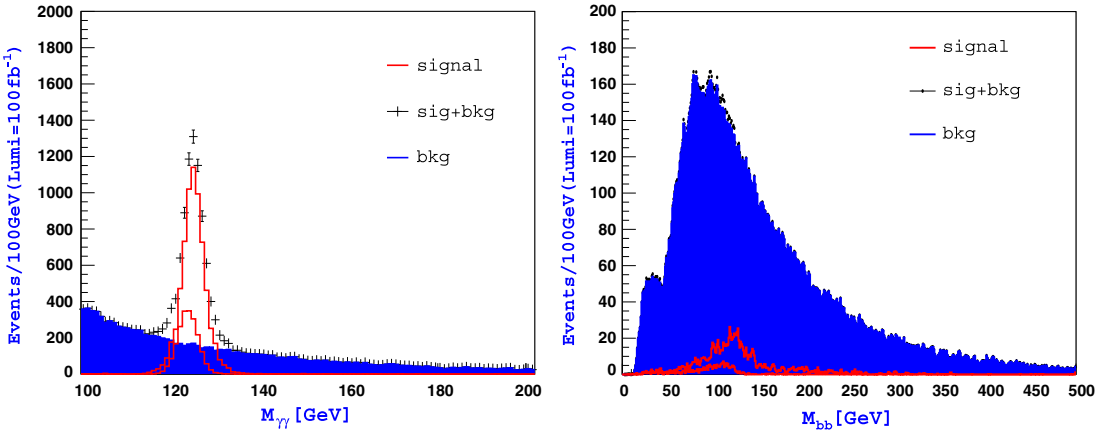

FIG. 5. Number of signal events for $h' \to \gamma\gamma b\bar{b}$ decays (red) induced by ggF and VBF versus the $\gamma\gamma$ (left) and $b\bar{b}$ (right) invariant mass at $\sqrt{s} = 13$ TeV after 100 fb^{-1} of luminosity alongside the total background (blue). Their sum is also shown as data points. Here, $m'_h = 300$ and 480 GeV. Only the acceptance cuts described in the text are used here.

(1) the pseudorapidity η of the two photons must fall within the geometric acceptance of the detector for photons, $|\eta| \leq 2.4$;
(2) the ratio between the transverse momenta of the leading and subleading photon must be ≥ 0.25;
(3) jets are required to fall within the tracker acceptance of $|\eta| \leq 2.5$ with transverse momentum $p_T \geq 35$ GeV.

After our preselection is enforced, already at the standard luminosity of Run 2, the signal is clearly visible above all backgrounds, both at 300 and 480 GeV, thereby enabling one to declare discovery of a Higgs-to-two-Higgs signal as well as circumstantial evidence of a BLSSM decay chain of the type $h' \to hh$. In order to eventually profile the latter though, the simultaneous reconstruction of the two h resonances and of the h' one is a prerequisite. To this end, in Fig. 5, we also show the mass reconstruction of the two SM-like Higgs boson masses, in the two channels $h \to \gamma\gamma$ and $b\bar{b}$, against the backdrop of the SM noise. From the corresponding distributions, a clear element emerges that characterizes this signature as very promising, i.e., the very efficient reconstruction of $m_h \approx 125$ GeV from the diphoton pair, from which is evident the strong background suppression that can be achieved. In contrast, this is not true in the case of $b\bar{b}$ decays, as here the background remains overwhelming above the signal (implicitly also explaining the reduced sensitivity of the fully hadronic $4b$ signal previously considered, where jet combinatorics would further play a significant role in degrading the quality of it). Furthermore, notice that the quality of the mass reconstruction is not dramatically different for $m_{h'} = 300$ and 480 GeV.

In the light of the mass distributions just discussed, one can attempt a more refined signal selection against the continuum noise. In Table I we show the number of events for signal and continuum background after each cut mentioned therein and Fig. 6 shows the final number of

TABLE I. Signal (for two h' mass values) and continuum background events in the $\gamma\gamma b\bar{b}$ channel as a function of several mass selection cuts. The energy is $\sqrt{s} = 13$ TeV, whereas the luminosity is 100 fb^{-1}.

Applied cut	Signal, $m_{h'} = 300$	Signal, $m_{h'} = 480$	Continuum background
After acceptance cuts	626	237	4758
$M_{\gamma\gamma} \leq 135$ GeV	625	234	4375
$M_{\gamma\gamma} \geq 115$ GeV	616	223	182
$M_{b\bar{b}} \leq 145$ GeV	536	210	98
$M_{b\bar{b}} \geq 105$ GeV	351	86	30

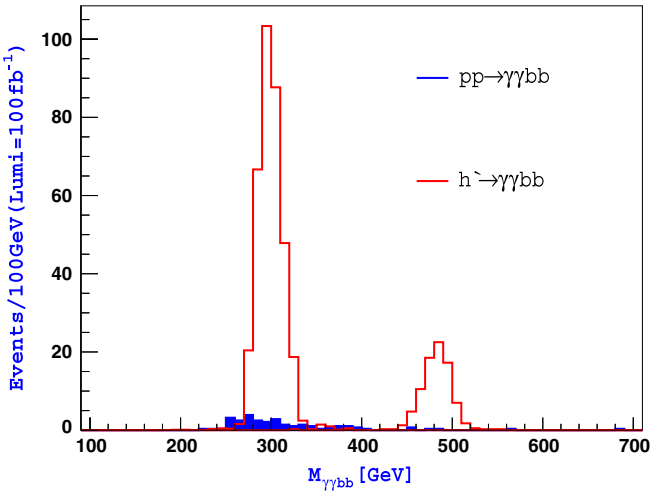

FIG. 6. Number of signal events for $h' \to \gamma\gamma b\bar{b}$ decays (red) induced by ggF and VBF versus the $\gamma\gamma$ invariant mass at $\sqrt{s} = 13$ TeV after 100 fb^{-1} of luminosity alongside the total background (blue). Here, $m'_h = 300$ and 480 GeV. Also the selection cuts of Table II are used here.

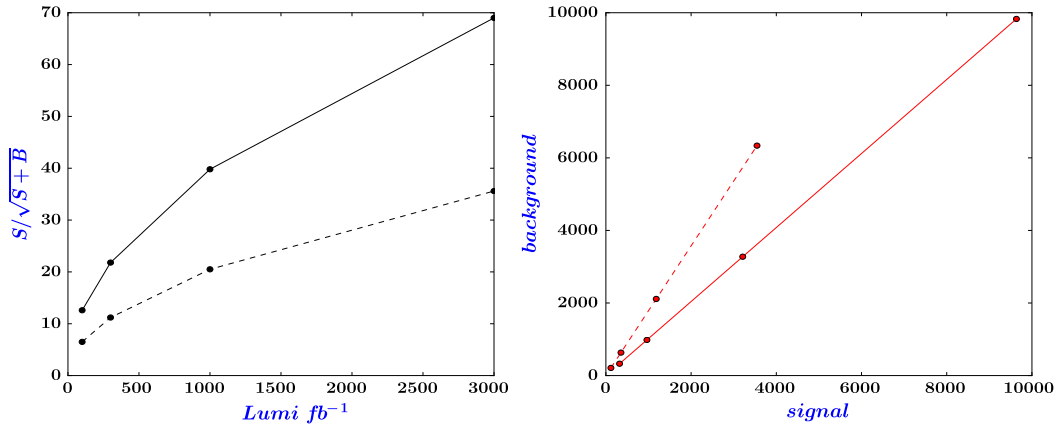

FIG. 7. Left: Significance of the $h' \to \gamma\gamma b\bar{b}$ signal (for $m_{h'} = 300$ and 480 GeV) versus the luminosity. Right: Number of events for signal and background for variable luminosity. Data are produced at $\sqrt{s} = 13$ TeV and the points correspond to an integrated luminosity of 100, 300, 1000, and 3000 fb^{-1}. Notice that event rates are computed after the acceptance cuts described in the text and the mass selections of Table II. The $M_{\gamma\gamma b\bar{b}}$ mass windows used for the calculation are 50 GeV for $m_{h'} = 300$ GeV and 100 GeV for $m_{h'} = 480$ GeV.

events versus the background after all cuts are applied. It is clear from this plot that the final result is an almost background-free $M_{\gamma\gamma b\bar{b}}$ distribution neatly pointing to the value of the h' mass, for values between 300 and 480 GeV. It is not surprising then, in the end, significances for the signal can be extremely large, as seen in Fig. 7, for any $m_{h'}$ value, after a final sampling in $M_{\gamma\gamma b\bar{b}}$ is exploited. Notice that, here, both reducible and irreducible backgrounds are accounted for in the calculation.

IV. SEARCH FOR A LIGHT BLSSM HIGGS BOSON AT THE LHC

In this section we briefly revisit the possible signatures of a light BLSSM Higgs boson h' (with mass $m_{h'} \approx 140$ GeV) at the LHC. As emphasized in Refs. [2–4], this particle can be probed in one of the following channels: $\gamma\gamma$, $Z\gamma$, and ZZ. We review these in the three upcoming subsections.

A. The $\gamma\gamma$ decays of a light BLSSM Higgs boson

The coupling of a Higgs boson with diphotons is induced by loops of charged particles. In the SM, these loops are mediated by the W gauge boson and top quark. In SUSY models, the $h\gamma\gamma$ triangle coupling contains additional loops of charged particles: charged Higgs bosons $H^{\pm}$, squarks $\tilde{q}$, sleptons $\tilde{\ell}^{\pm}$, and charginos $\chi^{\pm}$. Since the Higgs bosons coupling with SUSY particles are not proportional to their masses, their contributions decouple for high masses. In this paper, we focus on the cases of light chargino, $\chi_1^{\pm}$, enhancements, since they can increase the $h\gamma\gamma$ amplitude squared up to 30% [23,24] (i.e., the sfermions and charged Higgs bosons are assumed to be heavy).

The Higgs decay into diphotons provides a clean final-state topology that allows for the mass to be reconstructed with high precision. The partial decay width of the lightest BLSSM Higgs boson into diphotons is given by

$$\Gamma(h' \to \gamma\gamma) = \frac{G_\mu \alpha^2 m_{h'}^3}{128\sqrt{2}\pi^3} |A_t + A_W + A_{H^\pm} + A_{\tilde{f}} + A_{\chi^\pm}|^2, \tag{23}$$

where the amplitudes $A_{f,W,H^\pm,\tilde{f},\chi^\pm}$ can be found in [25]. In Fig. 8 we show the signal strength of $gg \to h' \to \gamma\gamma$ for 110 GeV $< m_{h'} <$ 150 GeV. We also include the diphoton signal strengths of the SM-like Higgs, h, in the MSSM and BLSSM, in addition to the MSSM-like heavy Higgs, H.

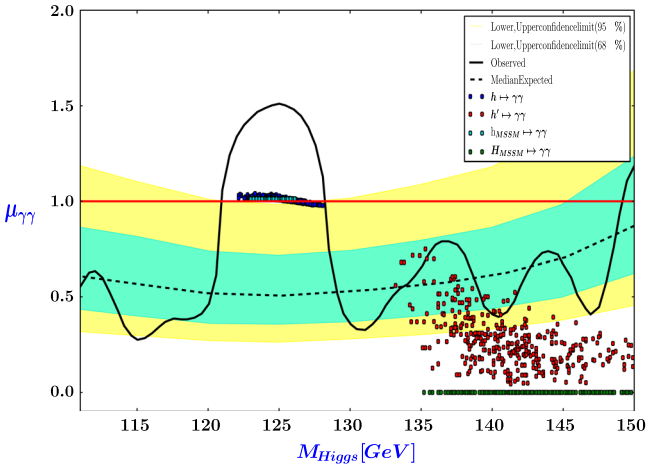

FIG. 8. Signal strength of the lightest and next-to-lightest Higgs bosons in the BLSSM (in blue and red, respectively) in the $\gamma\gamma$ channel. For comparison, we also include the signal strength of the lightest and next-to-lightest Higgs bosons in the MSSM (in cyan and black, respectively). The 1 and 2σ confidence intervals are extracted from data collected during Run 1 with the observed exclusion limit as given in [26] also included.

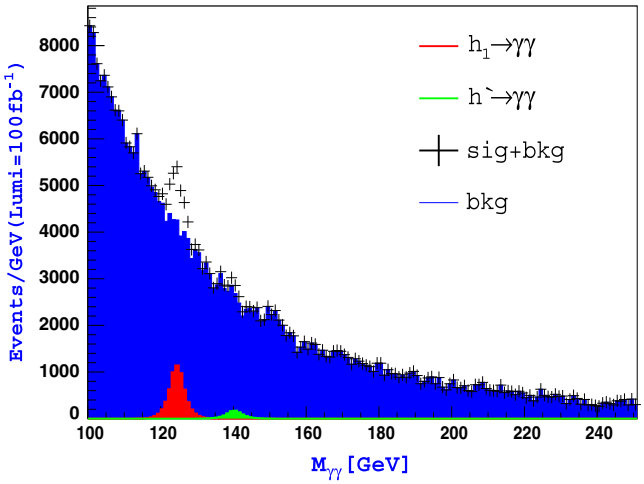

FIG. 9. Number of signal events for h and $h' \to \gamma\gamma$ decays (red and green, respectively) induced by ggF and VBF versus the $\gamma\gamma$ invariant mass at $\sqrt{s} = 13$ TeV after 100 fb^{-1} of luminosity alongside the total background (blue). Their sum is also shown as data points.

It is interesting to note that the BLSSM results for both h and h' match the observed data at Run 1, whereas the signal strength of the heavy Higgs in the MSSM, H, is quite suppressed and cannot easily account for these observations.

The number of events for $h' \to \gamma\gamma$ as a function of the diphoton invariant mass is presented in Fig. 9, for a center-of-mass (CM) energy $\sqrt{s} = 13$ TeV and integrated luminosity $= 100$ fb^{-1}. Here we choose the input parameters such that the SM-like Higgs boson has a mass $m_h = 125$ GeV and the lightest genuinely BLSSM Higgs state has a mass $m_{h'} \sim 140$ GeV. The dominant backgrounds consist of an irreducible fraction from prompt diphoton production and a reducible one from $\gamma +$ jet and dijet events where one or more of the objects reconstructed as a photon corresponds to a jet, according to CMS "fake rates." It is also worth mentioning that here we consider all cuts applied in the CMS analysis of Ref. [26]; i.e., the photon candidates are collected within $|\eta^\gamma| \leq 2.5$ with transverse momentum $p_T^\gamma \geq 20$ GeV. The production is considered here as induced from both ggF and VBF (as at higher energies the latter mode grows in importance relative to the former) and yield both a h and h' state. As can be seen from this figure, the peak at ∼140 GeV is greatly overwhelmed by the background after 100 fb^{-1}, yet is accessible with additional luminosity, as shown in Fig. 10.

B. The $Z(\to \ell^+\ell^-)\gamma$ decays of a light BLSSM Higgs boson

Despite its small BR, the LHC experiments are currently sensitive to this channel and will be so more and more as luminosity accrues. Precisely because the SM rate in this decay channel is small, ATLAS and CMS may access BSM physics through it, owing to the fact that the partial width can increase sizably in the presence of additional loops of charged particles, just like in the $h' \to \gamma\gamma$ channel. The partial decay width of the lightest BLSSM Higgs boson into $Z\gamma$ is given by

$$\Gamma(h' \to Z\gamma) = \frac{G_f^2 \alpha^2 M_W^2 M_{h'}^3}{64\pi^4}\left(1 - \frac{M_Z^2}{M_{h'}^2}\right)^3 |A_f + A_W + A_{H^\pm} + A_{\tilde{f}} + A_{\chi^\pm}|^2, \quad (24)$$

where the amplitudes $A_{f,W,H^\pm,\tilde{f},\chi^\pm}$ can be found in [27]. As discussed in [4], due to the mixing in the sfermion and chargino sectors, the diagonal coupling only enhances the $h' \to \gamma\gamma$ channel, while the fact that the Z boson has both vector and axial vector quantum numbers makes both diagonal and off-diagonal couplings of sfermions and charginos contribute to the $h' \to Z\gamma$ channel. As in

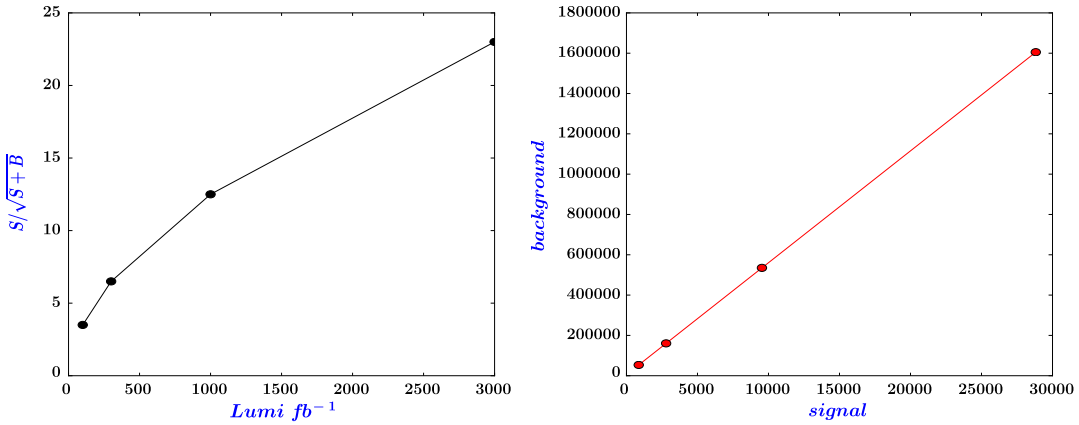

FIG. 10. Left: Significance of the $h' \to \gamma\gamma$ signal (for $m_{h'} = 140$ GeV) versus the luminosity. Right: Number of events for signal and background for variable luminosity. Data are produced at $\sqrt{s} = 13$ TeV and the points correspond to an integrated luminosity of 100, 300, 1000, and 3000 fb^{-1}. Notice that event rates are computed after the cut $|m_{\gamma\gamma} - m_{h'}| < 10$ GeV.

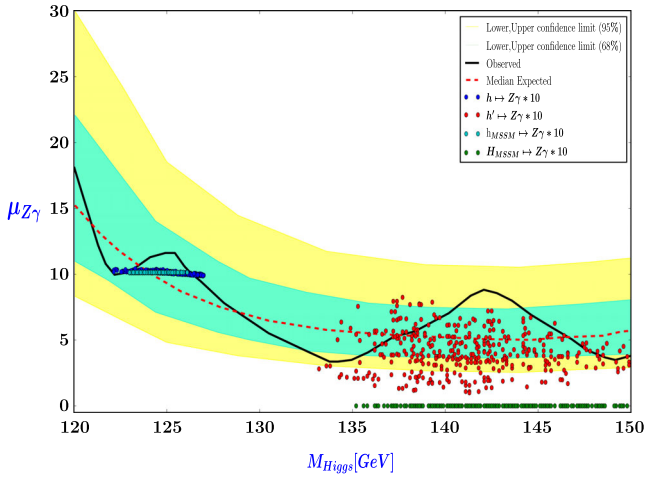

FIG. 11. Signal strength of the lightest and next-to-lightest Higgs bosons BLSSM (in blue and red, respectively) in the $Z\gamma$ channel. The signal strength of the lightest and next-to-lightest Higgs bosons in the MSSM are given in cyan and black points, respectively. The 1 and 2σ confidence intervals are extracted from data collected during Run 1 with the observed exclusion limit as given in [28] also included.

$h' \to \gamma\gamma$, we focus here on a light chargino in order to enhance the $h' \to Z\gamma$ amplitude.

In Fig. 11 we show that the signal strength of the h', h (both in the MSSM and BLSSM) and H decays to $Z\gamma$ for $m_{h',H}$ around 140 GeV (as usual, $m_h = 125$ GeV), with the 1 and 2σ confidence intervals extracted from data collected during Run 1 and with the observed exclusion limit as given in [28]. As can be seen, again, the BLSSM results for both h and h' match with the observed data rather well, whereas the signal strength of the heavy Higgs in the MSSM, H, as expected, is quite suppressed and hence unable to reach out to current experimental results.

TABLE II. Signal and background events in the $Z\gamma$ channel assuming electron and muon decays of the Z boson as a function of the selection cuts detailed in the text. The energy is $\sqrt{s} = 13$ TeV whereas the luminosity is 100 fb^{-1}.

	Signal (S)	Background (B)	$\frac{S}{\sqrt{S+B}}$
Before cuts	200	18828	1.44
$p_T^\gamma \geq 25$ GeV	180	6490	2.2
85 GeV $\leq M_{\ell^+\ell^-} \leq 95$ GeV	172	4500	2.5
130 GeV $\leq M_{\ell^+\ell^-\gamma} \leq 150$ GeV	170	3822	2.7

The distribution of the "dilepton + photon" (we assume $Z \to \ell^+\ell^-$, $\ell = e, \mu$) invariant mass is presented in Fig. 12 for the signal and background, where the dominant components of the latter consist of the irreducible contribution from $Z\gamma$ production and the reducible one from final-state radiation in the neutral Drell-Yan process and Z + jets processes where a jet is misidentified as a photon. Here the cuts applied are as in Ref. [28], i.e.,

(1) the photon pseudorapidity must be $|\eta^\gamma| \leq 2.5$;
(2) the photon transverse momentum must be $p_T^\gamma \geq 25$ GeV;
(3) the dilepton invariant mass must be 85 GeV $\leq M_{\ell^+\ell^-} \leq 95$ GeV;
(4) the dilepton + photon invariant mass must be 130 GeV $\leq M_{\ell^+\ell^-\gamma} \leq 150$ GeV.

The cut flow results are found in Table II. The selection (based on Run 1 cuts) remains effective at Run 2 as well, since already at standard luminosity there could already be evidence of the $h' \to Z\gamma$ signal in the BLSSM. The line shape of the signal, initially swamped by the background (see the left-hand side of Fig. 12), would also be very distinctive after the selection is enforced (see the right-hand side of Fig. 12). As the luminosity at Run 2 accumulates,

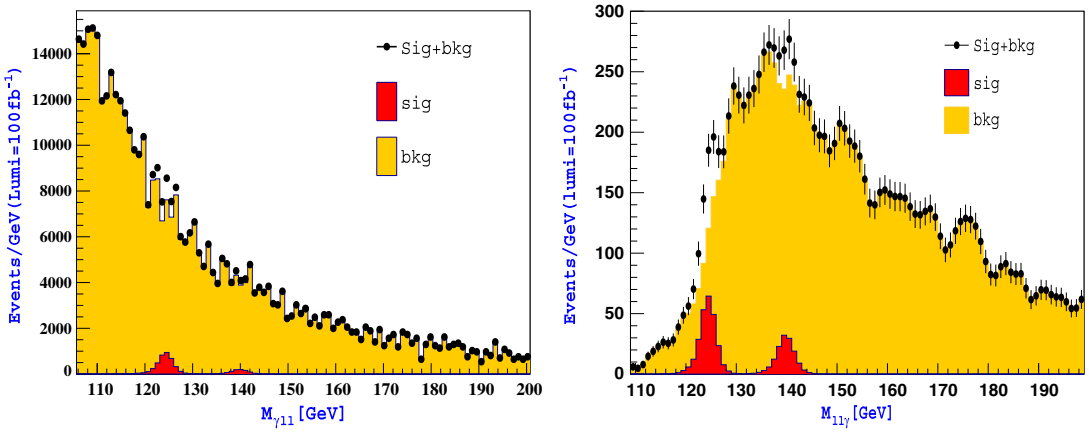

FIG. 12. Number of signal events for h and $h' \to Z(\to \ell^+\ell^-)\gamma$ decays ($\ell = e, \mu$) (red) induced by ggF and VBF versus the $\ell^+\ell^-\gamma$ invariant mass at $\sqrt{s} = 13$ TeV after 100 fb^{-1} of luminosity alongside the total background (yellow). Their sum is also shown as data points. Left: Before the cuts in the text are applied. Right: After.

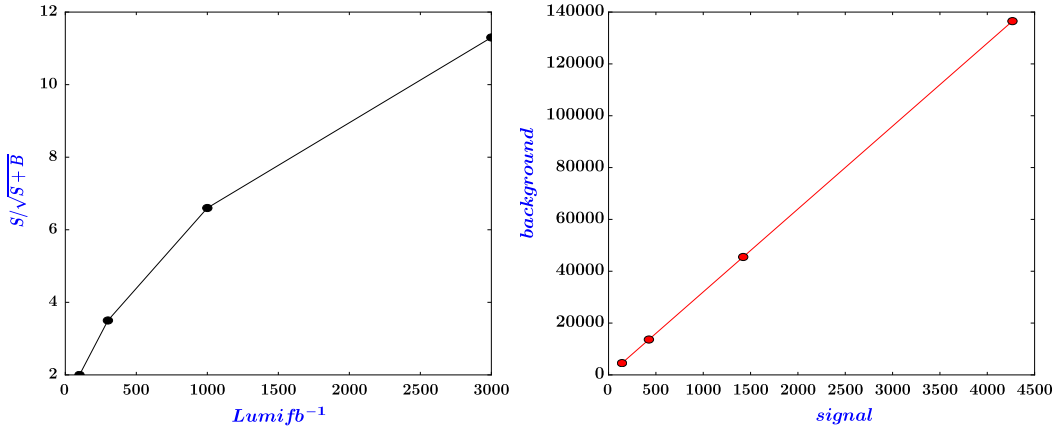

FIG. 13. Left: Significance of the $h' \to Z(\to \ell^+\ell^-)\gamma$ signal (for $m_{h'} = 140$ GeV and $\ell = e, \mu$) versus luminosity. Right: Number of events for signal and background for variable luminosity. Data are produced at $\sqrt{s} = 13$ TeV and the points correspond to an integrated luminosity of 100, 300, 1000, and 3000 fb^{-1}. Notice that event rates are computed after the cuts described in the text.

the evidence will eventually turn into clear discovery (see Fig. 13).

C. The $ZZ(\to 4\ell)$ decays of a light BLSSM Higgs boson

The four-lepton final state through the Higgs decay via pairs of Z bosons is the most significant channel for Higgs detection, yet it may not be the most sensitive one to BSM effects, as its leading contribution occurs at tree level, so that mixing effects of the SM-like boson with additional Higgs boson states typically drive the BSM deviations. It was however one of the channels in which an anomaly at around 140 GeV appeared following the Run 1 analyses, as intimated. In the MSSM, as mentioned above, in order to keep the signal strength of the lightest Higgs boson h consistent with the observed data, one is constrained to the decoupling region, where $M_A \gg M_Z$ and the Higgs mixing angle $\alpha \sim \beta - \frac{\pi}{2}$. Therefore, the coupling of the heaviest MSSM CP-even Higgs boson, H, with the SM gauge bosons is very suppressed. In the case of the BLSSM, $\tilde{g}$ plays an important role in enhancing both the lightest and the second-lightest CP-even Higgs boson couplings with SM gauge bosons, as discussed in [2] and seen in Fig. 1.

In Fig. 14, we show the signal strength of h and h' decays to ZZ for $m_h \approx 125$ GeV and $m_{h'}$ around 140 GeV along with 1 and 2σ confidence bands extracted from data collected during Run 1 with the observed exclusion limit of [28]. As the other two channels previously discussed, the results of the BLSSM for both h and h' match the observed data rather closely. We refrain from presenting here the

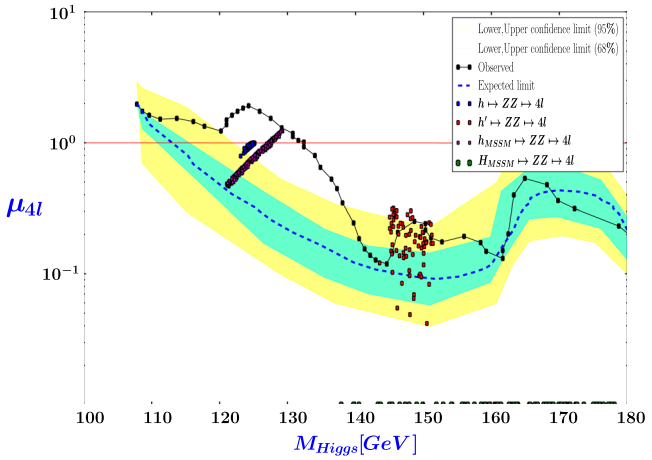

FIG. 14. Signal strength of the lightest and next-to-lightest Higgs bosons in the BLSSM (in blue and red, respectively) in the ZZ channel. The signal strength of the lightest and next-to-lightest Higgs bosons in the MSSM are given in violet and green points, respectively. The 1 and 2σ confidence intervals are extracted from data collected during Run 1 with the observed exclusion limit as given in [5] also included.

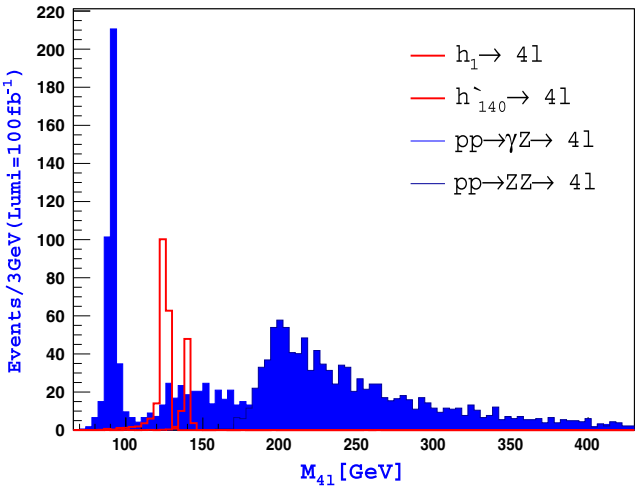

FIG. 15. Number of signal events for h and $h' \to ZZ(\to 4\ell)$ decays ($\ell = e, \mu$) (red) induced by ggF and VBF versus the 4ℓ invariant mass at $\sqrt{s} = 13$ TeV after 100 fb^{-1} of luminosity alongside the two dominant backgrounds (blue and black).

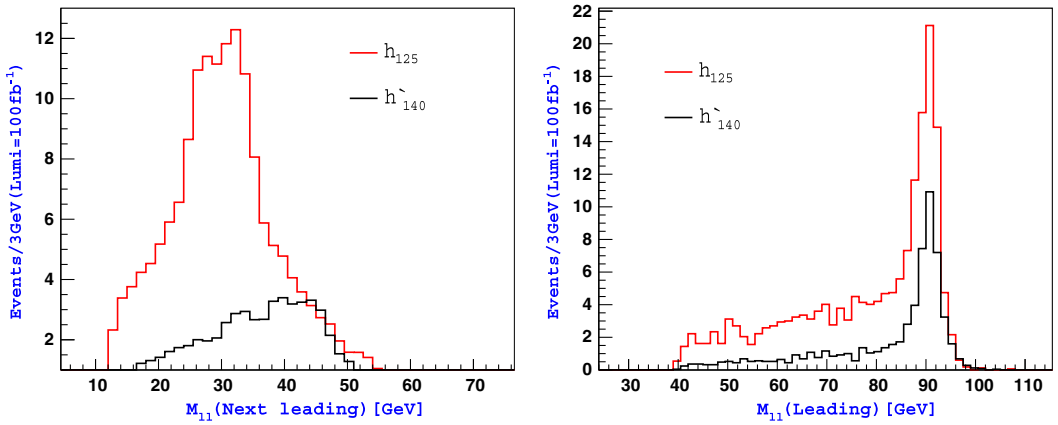

FIG. 16. Number of signal events for h (red) and $h' \to ZZ(\to 4\ell)$ (black) decays ($\ell = e, \mu$) induced by ggF and VBF versus the 2ℓ invariant mass at $\sqrt{s} = 13$ TeV after 100 fb^{-1} of luminosity. Left: Off-shell Z case. Right: On-shell Z case.

MSSM results for h as in the decoupling limit they essentially coincide with the SM ones (whereas those for the MSSM H boson are outside the frame).

The results of our simulation for Run 2 are based on $ZZ \to 4\ell$ decays, wherein $\ell = e, \mu$. In Fig. 15, we show the number of events for the h and h' bosons in the BLSSM plotted against the four-lepton invariant mass. As can be seen from this plot, a promising signature of $h' \to ZZ \to 4\ell$ around 140 GeV emerges alongside the SM-like one at ≈125 GeV. The main contributions from SM backgrounds come from $Z\gamma^*$ and $ZZ^{(*)}$. Significances at 100 fb^{-1} are already enough to claim evidence in both Higgs channels.

Reconstruction of the h and h' decays can only be performed for one on-shell (Z) and one off-shell (Z^*) gauge boson, as $M_Z < m_{h,h'} < 2M_Z$ for both Higgs states. We notice that the combination of the two highest p_T leptons is the most likely one to emerge from the on-shell Z boson decay while the other two leptons most often come from the off-shell Z boson decay. Figure 16 shows the reconstruction of both the off-shell and on-shell Z boson decays for both h and h', illustrating that the off-shell distribution can be used to increase the purity of each signal from cross-contamination.

In the light of such Z boson spectra, we required the following cuts.

(1) The pseudorapidity of both electrons and muons is $|\eta| \leq 2.5$.
(2) We require a Z candidate formed with a pair of leptons of the same flavor and opposite charge, with mass window $40 \leq M_Z \leq 120$ GeV, the remaining leptons constructing the second off-shell Z boson if they satisfy $12 \leq M_Z \leq 120$ GeV.
(3) In reconstructing the on-shell Z we require the highest transverse momentum lepton pair to be ≥ 20 GeV.
(4) To protect the signals against leptons originating from hadron decays in jet fragmentation or from the decay of low-mass hadronic resonances, we require

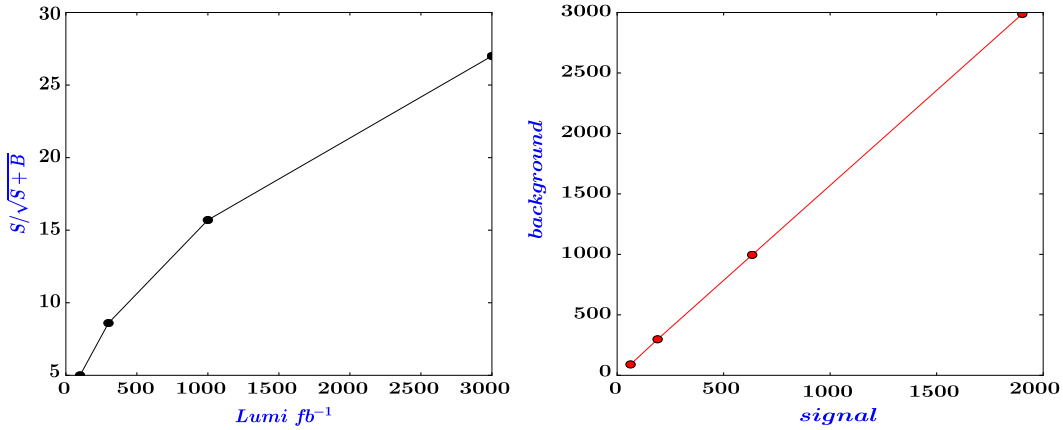

FIG. 17. Left: Significance of the $h' \to ZZ(\to 4\ell)$ signal (for $m_{h'} = 140$ GeV and $\ell = e, \mu$) versus the luminosity. Right: Number of events for signal and background for variable luminosity. Data are produced at $\sqrt{s} = 13$ TeV and the points correspond to an integrated luminosity of 100, 300, 1000, and 3000 fb^{-1}. Notice that event rates are computed after the cuts described in the text.

$M_{\ell^+\ell^-} \geq 4$ GeV, where $M_{\ell^+\ell^-}$ is the invariant mass of any lepton pair.

Such a selection is already effective at 100 fb^{-1} and, as usual, increasing luminosity will render this signal more and more significant, as per trend seen in Fig. 17.

V. CONCLUSION

We have analyzed the discovery potential of a second neutral Higgs boson in the BLSSM at the LHC. We have confirmed that a double Higgs peak structure can be accessed in this framework, in the $\gamma\gamma$, $Z(\to \ell^+\ell^-)\gamma$, and $ZZ(\to 4\ell)$ decay channels with Higgs boson masses at $m_h \sim 125$ GeV and $m_{h'} = 140$ GeV, wherein h and h' are the lightest CP-even Higgs states of the MSSM-like and genuine BLSSM spectra, respectively.

Furthermore, under the assumption that the aforementioned excesses are not confirmed by Run 2 data, we have studied the possibilities at the CERN machine of establishing signals of a heavier h' state of the BLSSM. We have shown that a peculiar decay in the BLSSM is $h' \to hh$ (i.e., into a pair of SM-like Higgs bosons), which can in fact be dominant from its threshold (at $m_{h'} \approx 2m_h \approx 250$ GeV) onwards. We have shown that the associate $\gamma\gamma b\bar{b}$ signature can be spectacularly visible over a wide mass interval, from, say, 250 to 500 GeV.

Combining all these results, and noting that similar Higgs signals would not be available in the MSSM, we conclude that their extraction, either around 140 GeV or anywhere beyond 250 GeV or so, would not only point to a nonminimal SUSY scenario, hence beyond the MSSM, but also possibly pinpoint the BLSSM.

ACKNOWLEDGMENTS

S. K. is partially supported by the STDF Project No. 13858. S. M. is supported in part through the NExT Institute. All authors acknowledge support from Grant No. H2020-MSCA-RISE-2014 No. 645722 (NonMinimalHiggs). A. H. is partially supported by the EENP2 FP7-PEOPLE-2012-IRSES grant.

[1] We conventionally denote here by $A^{(\prime)}$ CP-odd Higgs states and by $h^{(\prime)}, H^{(\prime)}$ CP-even ones (the latter with $m_h < m_H$ and $m_{h'} < m_{H'}$). Notice also that two charge conjugated states are present in both the MSSM and BLSSM, denoted by $H^{\pm}$.
[2] W. Abdallah, S. Khalil, and S. Moretti, Double Higgs peak in the minimal SUSY B-L model, Phys. Rev. D **91**, 014001 (2015).
[3] S. Khalil and S. Moretti, Can we have another light (∼145 GeV) Higgs boson?, arXiv:1510.05934.
[4] A. Hammad, S. Khalil, and S. Moretti, Higgs boson decays into $\gamma\gamma$ and $Z\gamma$ in the MSSM and BLSSM, Phys. Rev. D **92**, 095008 (2015).
[5] CMS Collaboration, Measurement of the properties of a Higgs boson in the four-lepton final state, Phys. Rev. D **89**, 092007 (2014).
[6] CMS Collaboration, Report Nos. CMS-PAS-HIG-13-001 and CMS-PAS-HIG-13-016, 2013.
[7] CMS Collaboration, Search for a Higgs boson decaying into a Z and a photon in pp collisions at $\sqrt{s} = 7$ and 8 TeV, Phys. Lett. B **726**, 587 (2013).
[8] S. Khalil and A. Masiero, Radiative B-L symmetry breaking in supersymmetric models, Phys. Lett. B **665**, 374 (2008).
[9] F. Staub, Exploring new models in all detail with SARAH, Adv. High Energy Phys. **2015**, 840780 (2015).
[10] Hereafter, the bulk of the production rates will be due to the first two channels.
[11] F. Staub, SARAH 4: A tool for (not only SUSY) model builders, Comput. Phys. Commun. **185**, 1773 (2014).
[12] W. Porod and F. Staub, SPheno 3.1: Extensions including flavour, CP-phases and models beyond the MSSM, Comput. Phys. Commun. **183**, 2458 (2012).
[13] J. S. Lee, M. Carena, J. Ellis, A. Pilaftsis, and C. E. M. Wagner, CPsuperH2.3: An updated tool for phenomenology in the MSSM with explicit CP violation, Comput. Phys. Commun. **184**, 1220 (2013).
[14] J. Alwall, M. Herquet, F. Maltoni, O. Mattelaer, and T. Stelzer, MadGraph 5: Going Beyond, J. High Energy Phys. 06 (2011) 128.
[15] T. Sjostrand, S. Mrenna, and P. Z. Skands, A brief introduction to PYTHIA 8.1, Comput. Phys. Commun. **178**, 852 (2008).
[16] J. de Favereau, C. Delaere, P. Demin, A. Giammanco, V. Lemaître, A. Mertens, and M. Selvaggi (DELPHES 3 Collaboration), DELPHES 3: A modular framework for fast simulation of a generic collider experiment, J. High Energy Phys. 02 (2014) 057.
[17] E. Conte, B. Fuks, and G. Serret, MadAnalysis 5: A user-friendly framework for collider phenomenology, Comput. Phys. Commun. **184**, 222 (2013).
[18] ATLAS Collaboration, A search for resonant Higgs-pair production in the $b\bar{b}b\bar{b}$ final state in pp collisions at $\sqrt{s} = 8$ TeV, Report No. ATLAS-CONF-2014-005.
[19] CMS Collaboration, Search for di-Higgs resonances decaying to 4 bottom quarks, Report No. CMS-PAS-HIG-14-013.
[20] G. Aad *et al.* (ATLAS Collaboration), Search for Higgs Boson Pair Production in the $\gamma\gamma b\bar{b}$ Final State Using pp Collision Data at $\sqrt{s} = 8$ TeV from the ATLAS Detector, Phys. Rev. Lett. **114**, 081802 (2015).
[21] CMS Collaboration, Search for the resonant production of two Higgs bosons in the final state with two photons and two bottom quarks, Report No. CMS-PAS-HIG-13-032.

[22] G. Aad *et al.* (ATLAS Collaboration), Search for Higgs boson pair production in the $b\bar{b}b\bar{b}$ final state from pp collisions at $\sqrt{s} = 8$ TeV with the ATLAS detector, Eur. Phys. J. C **75**, 412 (2015).

[23] A. Belyaev, S. Khalil, S. Moretti, and M. C. Thomas, Light sfermion interplay in the 125 GeV MSSM Higgs production and decay at the LHC, J. High Energy Phys. 05 (2014) 076.

[24] M. Hemeda, S. Khalil, and S. Moretti, Light chargino effects onto $H \to \gamma\gamma$ in the MSSM, Phys. Rev. D **89**, 011701 (2014).

[25] A. Djouadi, The anatomy of electro-weak symmetry breaking. II. The Higgs bosons in the minimal supersymmetric model, Phys. Rep. **459**, 1 (2008).

[26] G. Aad *et al.* (ATLAS Collaboration), Measurement of Higgs boson production in the diphoton decay channel in pp collisions at center-of-mass energies of 7 and 8 TeV with the ATLAS detector, Phys. Rev. D **90**, 112015 (2014).

[27] A. Djouadi, V. Driesen, W. Hollik, and A. Kraft, The Higgs photon–Z boson coupling revisited, Eur. Phys. J. C **1**, 163 (1998).

[28] G. Aad *et al.* (ATLAS Collaboration), Search for Higgs boson decays to a photon and a Z boson in pp collisions at $\sqrt{s} = 7$ and 8 TeV with the ATLAS detector, Phys. Lett. B **732**, 8 (2014).